Zero-Temperature Magnetic Properties of the Hubbard Model with Infinite Coulomb Repulsion*

J. S. Meyer and J. W. Schweitzer
Department of Physics and Astronomy, The University of Iowa, Iowa City, Iowa 52242
(Received 18 September 1972)

The two-pole approximation due to Roth for electron correlation in a narrow s band is applied to ferromagnetic and antiferromagnetic symmetries in simple cubic (sc) and body-centered-cubic (bcc) crystal structures and to ferromagnetic symmetry in the face-centered-cubic (fcc) structure. Numerical results in the case of zero-temperature, infinite-Coulomb-repulsion, and tight-binding nearest-neighbor band structures are presented. When the number of electrons is less than the number of sites, the paramagnetic susceptibilities of wave numbers corresponding to both magnetic symmetries exhibit two singularities as a function of electron concentration for both the sc and bcc structures, while there is no zero-wave-number singularity for the fcc structure. When the number of electrons is greater than the number of sites, there are two zero-wave-number singularities for the fcc structure and also, as a consequence of the electron-hole symmetry, there are two singularities for the sc and bcc structures. Magnetizations and energies are calculated for the various magnetic solutions as a function of electron concentration. Where it exists, the ferromagnetic solution having maximum total spin has the lowest energy. These results are in agreement with Nagaoka's conclusions for almost half-filled bands in the infinite-Coulomb-repulsion limit.

I. INTRODUCTION

In this work a numerical study of the magnetic properties of the narrow-s-band model within the two-pole approximation of Roth[1] is presented. The approximation is applied at zero temperature to narrow s bands modeled by nearest-neighbor tight-binding band structures in the limit that the Coulomb interaction between electrons of antiparallel spin associated with the same lattice site is infinite. Only ferromagnetic and antiferromagnetic configurations are considered.

In Sec. II the model Hamiltonian for the electronic system is presented. The static paramagnetic susceptibilities are calculated in Sec. III, and two instabilities toward both ferromagnetism and antiferromagnetism are found for both simple-cubic (sc) and body-centered-cubic (bcc) lattices. Instabilities toward ferromagnetism in the case of face-centered-cubic (fcc) lattices exist only when the number of electrons per site is greater than one. The calculation of the magnetization is presented in Sec. IV. In Sec. V, the relative energies of the configurations studied are presented. The lowest-energy configuration corresponds to the ferromagnetic phase of largest total spin, an extrapolation of the exact result obtained by Nagaoka[2] for the nearly half-filled band. In contrast, of the two antiferromagnetic configurations calculated for each lattice, the lowest energy corresponds to the phase with the smallest sublattice magnetization. In Sec. VI the results are discussed.

II. MODEL HAMILTONIAN

The model considered is the Hubbard Hamiltonian[3] for a narrow s band specialized to nearest-neighbor tight-binding band structures:

$$H = t \sum_{ij}^{nn} \sum_{\sigma} c_{i\sigma}^{\dagger} c_{j\sigma} + \tfrac{1}{2} I \sum_{i} \sum_{\sigma} n_{i\sigma} n_{i-\sigma} . \tag{1}$$

Here t is the transfer energy between states at neighboring sites, and I is the repulsive Coulomb energy for two electrons of antiparallel spin at the same site. The one-electron band energies are defined by

$$\epsilon_k = t \sum_{i}^{nn} e^{i\vec{k}\cdot\vec{R}_i} , \tag{2}$$

where $\vec{R}_i$ labels lattice sites. (The marking of vectors in indices will be suppressed throughout the paper.) The limit of infinite I will be assumed in what follows.

The expectation values of the Hamiltonian and the number operators $n_{i\sigma}$ are calculated from one-electron Green's functions.[4] The prescription used to obtain approximate expressions for these Green's functions is due to Roth.[1] A complete discussion of the application of the technique as applied to ferromagnetism is presented in Ref. 1. However, the formalism presented by Faulkner and Schweitzer[5] is more easily adapted for this study. Their results may be adopted for both magnetic symmetries with only a trivial specialization. The Fourier energy transform of the propagator is found to be the solution of

$$G_{ij}^{\sigma}(\omega) = G_i^{\sigma}(\omega)\delta_{ij} + G_i^{\sigma}(\omega)\, t \sum_{l}^{\text{nn of } i} G_{lj}^{\sigma}(\omega), \tag{3}$$

where

$$G_i^{\sigma}(\omega) = (1 - \bar{n}_{i-\sigma})(\omega - E_{i-\sigma})^{-1}, \tag{4}$$

with

$$\bar{n}_{i\sigma} = \langle n_{i\sigma} \rangle, \tag{5}$$

$$E_{i\sigma} = -t \sum_{j}^{\text{nn of } i} \langle C_{i\sigma}^{\dagger} C_{j\sigma} \rangle (1-\bar{n}_{i\sigma})^{-1} . \quad (6)$$

Equation (4) holds only when the number of electrons per site is less than one. This restriction is without loss of generality since the electron-hole symmetry of the model under the change in sign of t can be exploited to extend the results to the case where the number of electrons is greater than the number of sites.[2]

III. STATIC PARAMAGNETIC SUSCEPTIBILITY

The static paramagnetic susceptibility $\chi(\vec{q})$ becoming infinite signals the possibility of spontaneous magnetization with spatial variation characterized by $\vec{q}$. In particular, ferromagnetism is characterized by $\vec{q}=0$, while antiferromagnetism is characterized by $\vec{q}=\pi(1,1,1)$ for the sc lattice and by $\vec{q}=2\pi(1,1,1)$ for the bcc lattice. For the case of the two-pole approximation with infinite I, Schweitzer and Maynard[6] have given an explicit expression for $\chi(\vec{q})$. This expression is very lengthy and will not be reproduced here. However, at zero temperature the expression simplifies considerably for the values of $\vec{q}$ and the band structures considered in this work.

For $\vec{q}=0$, the inverse susceptibility is given by

$$\frac{(g\mu_B)^2}{2}\chi^{-1}(0) = \frac{1-2\bar{n}}{(1-\bar{n})\rho(\zeta)} + \zeta\left(1+\frac{1-2\bar{n}}{(1-\bar{n})^2}\right) + \frac{2}{1-\bar{n}}\int_{-\infty}^{\zeta} \epsilon\rho(\epsilon)\,d\epsilon . \quad (7)$$

For $\vec{q}=\vec{q}_A$, where $\vec{q}_A$ equals $\pi(1,1,1)$ for sc and $2\pi(1,1,1)$ for bcc lattices, we find using the fact that $\epsilon_{k+q_A} = -\epsilon_k$,

$$\frac{(g\mu_B)^2}{2}\chi^{-1}(\vec{q}_A) = \frac{1}{1-\bar{n}}\int_{-\infty}^{\zeta} \epsilon\rho(\epsilon)\,d\epsilon - \frac{1-2\bar{n}}{(1-\bar{n})^2}\left(\int_{-\infty}^{\zeta}\frac{\rho(\epsilon)\,d\epsilon}{\epsilon}\right)^{-1} . \quad (8)$$

Here $\bar{n}=\bar{n}_\sigma=\bar{n}_{-\sigma}$, ζ is the Fermi energy, and $\rho(\epsilon)$ is the density of states associated with ϵ_k defined by Eq. (2) and is assumed to be normalized to unity. The density-of-states curves[7] for the three lattice types are shown in Fig. 1 where we have chosen the transfer energy t in Eq. (2) to be equal to $-\frac{1}{2}$, $-\frac{1}{4}$, and $-\frac{1}{8}$ for the sc, fcc, and bcc crystal structures, respectively. The Eqs. (7) and (8) are restricted to the range of $\bar{n}$ where $2\bar{n}<1$; however, if one replaces everywhere $\rho(\epsilon)$ by $\rho(-\epsilon)$, then these expressions for χ^{-1} give the inverse susceptibility for $\bar{n}$ holes provided the number of electrons is greater than the number of sites. This follows from the electron-hole symmetry effected by changing the sign of t.

The curves for the inverse susceptibility versus the number of electrons per site ($n=2\bar{n}$) are shown in Figs. 2 and 3 for sc and bcc lattices, respectively. Since the susceptibilities are symmetric about $n=1$, only the values for $n<1$ are shown. In Fig. 4 the curve of $\chi^{-1}(0)$ for the fcc lattice is plotted for the entire range of electron concentration. Only the positive values of χ^{-1} are plotted in each of the three figures. Note that the sc and bcc lattices exhibit an instability toward ferromagnetism and also antiferromagnetism for *two* values of the electron concentration for $n<1$ (and, of course, also for $n>1$). The fcc lattice, while exhibiting no instability toward ferromagnetism for $n<1$, exhibits an instability at $n=1.2$ and another at $n=2$.

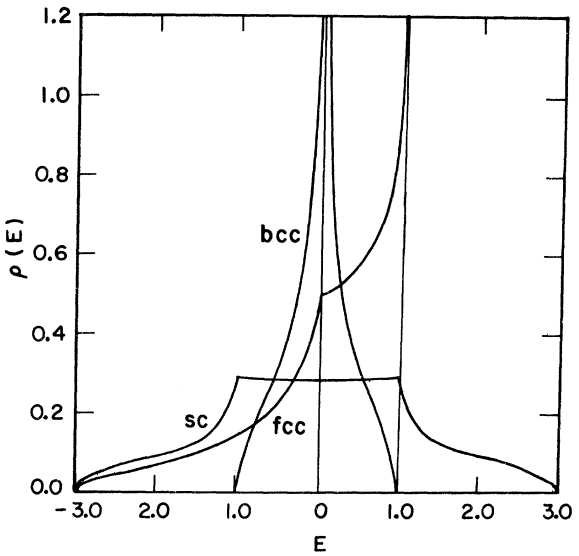

FIG. 1. Tight-binding nearest-neighbor density of states for simple-cubic, body-centered-cubic, and face-centered-cubic structures as a function of energy. All densities have been normalized to unity.

The fact that the susceptibility becomes infinite at two values of the electron concentration is a novel feature which suggests the possibility of two distinct ferromagnetic (antiferromagnetic) solutions at a given electron concentration. That this is indeed the case will be seen in Sec. IV.

IV. MAGNETIZATION

A. Ferromagnetism

For ferromagnetic solutions (i.e., $\bar{n}_{i\sigma}=\bar{n}_\sigma$, independent of the site) the Green's functions $G_{ij}^{\sigma}(\omega)$ depend only on the difference $\vec{R}_i - \vec{R}_j$. Hence the set of equations for $G_{ij}^{\sigma}(\omega)$ given by Eq. (3) is easily solved by introducing $G^{\sigma}(\vec{k},\omega)$ defined by

$$G_{ij}^{\sigma}(\omega) = N^{-1}\sum_{k} G^{\sigma}(\vec{k},\omega) e^{i\vec{k}\cdot(\vec{R}_i - \vec{R}_j)} , \quad (9)$$

where $\vec{k}$ is summed over the first Brillouin zone

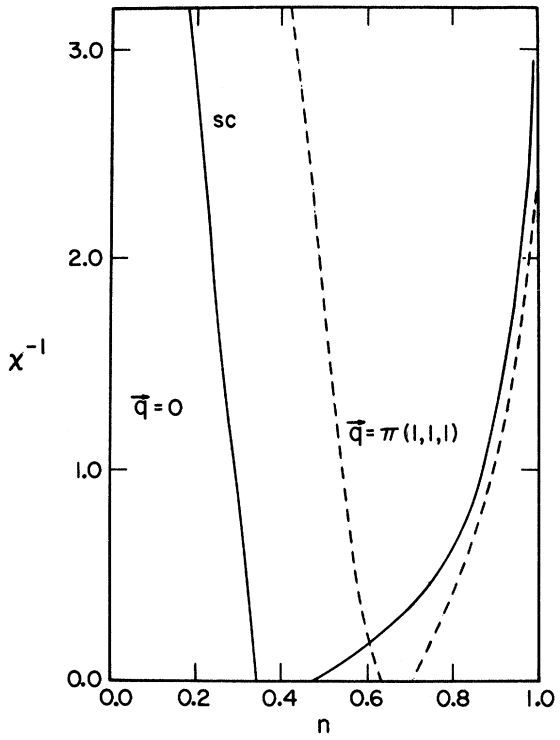

FIG. 2. Inverse static paramagnetic susceptibility of a simple-cubic lattice at absolute zero as a function of electron concentration. The ferromagnetic symmetry is represented by the $\vec{q}=0$ curve; the antiferromagnetic by $\vec{q}=\pi(1,1,1)$. Negative values are not plotted. Units are arbitrary.

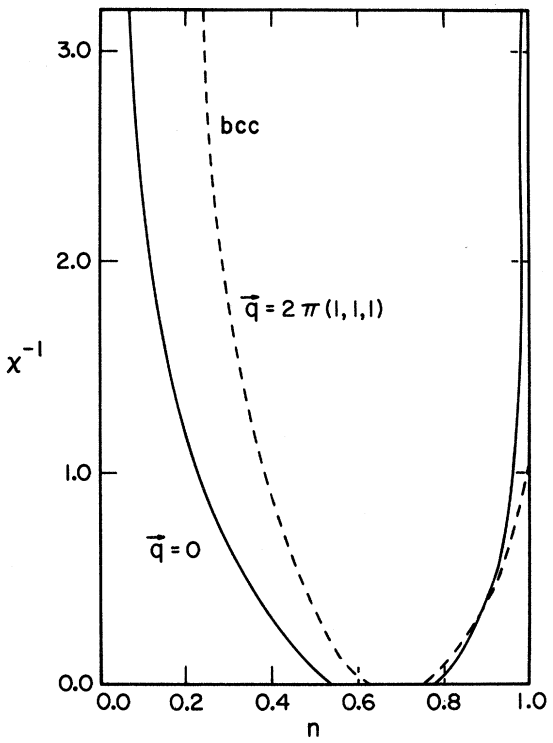

FIG. 3. Inverse static paramagnetic susceptibility of a body-centered-cubic lattice at absolute zero as a function of electron concentration. The ferromagnetic symmetry is represented by the $\vec{q}=0$ curve; the antiferromagnetic by $\vec{q}=2\pi(1,1,1)$. Negative values are not plotted. Units are arbitrary.

appropriate to the crystal lattice. Equation (3) yields

$$G^{\sigma}(\vec{k},\omega)=G^{\sigma}(\omega)[1-\epsilon_k G^{\sigma}(\omega)]^{-1}\ . \tag{10}$$

Here we have dropped the subscript on $G_i^{\sigma}(\omega)$ as defined by Eq. (4) since it does not now depend on the particular lattice site. The averages $\langle c_{i\sigma}^{\dagger} c_{j\sigma}\rangle$ are evaluated by the standard Green's-function

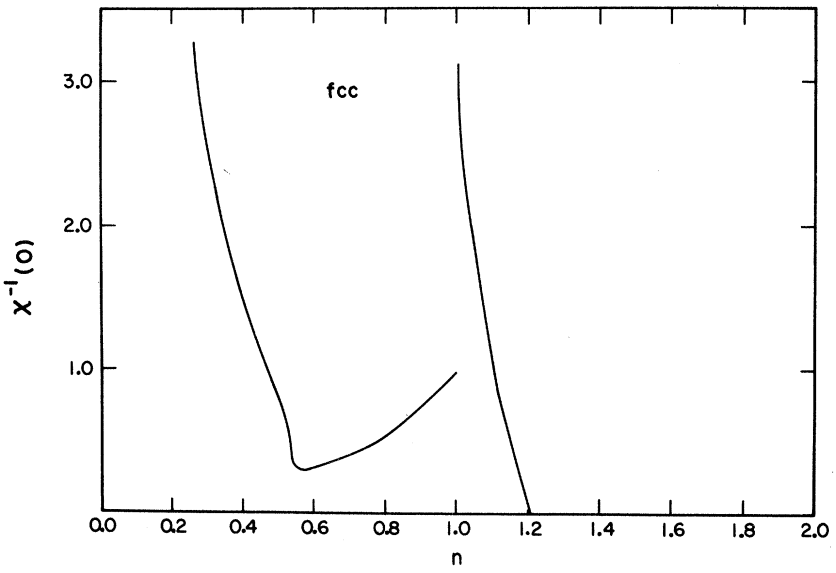

FIG. 4. Inverse static paramagnetic susceptibility of a face-centered-cubic lattice for $\vec{q}=0$ as a function of electron concentration. Negative values are not plotted. Units are arbitrary.

method.

At zero temperature this yields the set of self-consistency relations

$$\bar{n}_\sigma = (1-\bar{n}_{-\sigma})N^{-1}\sum_k \theta(\zeta - [E_{-\sigma} + (1-\bar{n}_{-\sigma})\epsilon_k]), \quad (11)$$

$$(1-\bar{n}_\sigma)E_\sigma = -(1-\bar{n}_{-\sigma})N^{-1}\sum_k \epsilon_k\,\theta(\zeta - [E_{-\sigma} + (1-\bar{n}_{-\sigma})\epsilon_k]), \quad (12)$$

where ζ is the Fermi energy and $\theta(x)$ is the heaviside unit function. The magnetization ($m = |\bar{n}_\sigma - \bar{n}_{-\sigma}|$) versus electron concentration ($n = \bar{n}_\sigma + \bar{n}_{-\sigma}$) curves are plotted in Figs. 5–7 for the sc, bcc, and fcc crystal structures. For the fcc structure there are only paramagnetic solutions when $n < 1$, in agreement with the susceptibility. For the sc and bcc structures the magnetization curves are symmetric about $n = 1$.

The most distinctive feature of these results is the existence of two ferromagnetic solutions. The one corresponding to the larger magnetization becomes saturated ($m = n$) for n sufficiently near the half-filled-band limit. The fcc results are exceptional in this respect. The logarithmic singularity in the density of states at the band edge is responsible for the saturated solutions throughout the range of n greater than one.

A similar calculation for the sc structure may be found in Ref. 1, and one is referred there for details on the method used to find solutions to Eqs. (11) and (12). However, there only the magnetization curve corresponding to the one in Fig. 5 with maximum magnetization was presented.

B. Antiferromagnetism

The Green's functions $G^\sigma_{ij}(\omega)$ for antiferromagnetic solutions will depend on the difference $\vec{R}_i - \vec{R}_j$ only if $\vec{R}_i$ and $\vec{R}_j$ belong to the same magnetic sublattice. In that case one can introduce $G^\sigma_S(\vec{k}, \omega)$ defined by

$$G^\sigma_{Si,Sj}(\omega) = 2N^{-1}\sum_k{}' G^\sigma_S(\vec{k}, \omega)e^{i\vec{k}\cdot(\vec{R}_{Si}-\vec{R}_{Sj})}, \quad (13)$$

where the subscript Si labels a site on the sublattice S. The prime on the summation symbol is to indicate that the sum is over the first Brillouin zone appropriate to the sublattice. The antiferromagnetic solutions are by definition

$$\bar{n}_{S,\sigma} = \bar{n}_{-S,-\sigma}, \quad (14)$$

where S and $-S$ denote the two sublattices. Since there is the symmetry between interchange of sub-

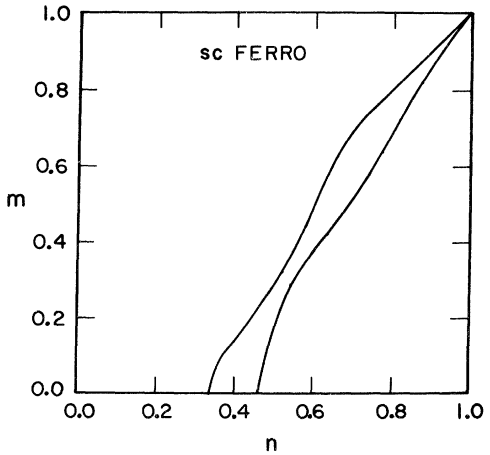

FIG. 5. Magnetization per site at absolute zero as a function of electron concentration for the simple-cubic lattice.

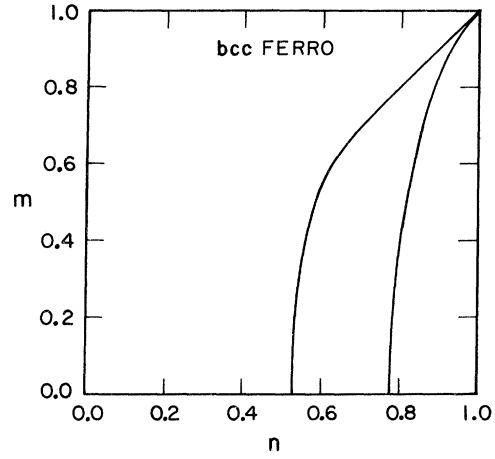

FIG. 6. Magnetization per site at absolute zero as a function of electron concentration for the body-centered-cubic lattice.

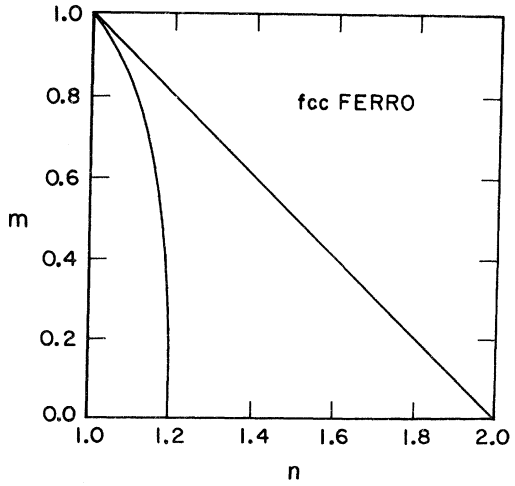

FIG. 7. Magnetization per site at absolute zero as a function of electron concentration for the face-centered-cubic lattice. No magnetic solutions occur until the band is half-filled.

lattice and interchange of spin orientation, the sublattice label may be suppressed.

Since our model has only nearest-neighbor transfer terms, the set of equations given in Eq. (3) easily decouples for the two sublattices. One finds

$$G^{\sigma}(\vec{k},\omega) = G^{\sigma}(\omega)\left[1 - \epsilon_k^2 G^{\sigma}(\omega)\, G^{-\sigma}(\omega)\right]^{-1}, \tag{15}$$

where $G^{\sigma}(\omega)$ is given by Eq. (4) provided the number of electrons per site is less than one. The expectation values $\langle c_{i\sigma}^{\dagger} c_{j\sigma}\rangle$ are evaluated using the standard Green's-function technique. The resulting self-consistency conditions for the electron concentration n, the sublattice magnetization $m = |\bar{n}_{\sigma} - \bar{n}_{-\sigma}|$, and a quantity α are given by the following at zero temperature and for $n < 1$:

$$n = (2-n)X_1 + mX_2, \tag{16}$$

$$m = mX_1 + (2-n)X_2, \tag{17}$$

$$\alpha = mX_3, \tag{18}$$

where

$$X_1 = N^{-1}\sum_k{}' \left[\theta\left(\zeta - \frac{2-n}{m}\,\alpha + R_k\right) + \theta\left(\zeta - \frac{2-n}{m}\,\alpha - R_k\right)\right], \tag{19}$$

$$X_2 = N^{-1}\sum_k{}' \frac{\alpha}{R_k}\left[\theta\left(\zeta - \frac{2-n}{m}\,\alpha + R_k\right) - \theta\left(\zeta - \frac{2-n}{m}\,\alpha - R_k\right)\right], \tag{20}$$

$$X_3 = N^{-1}\sum_k{}' \frac{\epsilon_k^2}{2R_k}\left[\theta\left(\zeta - \frac{2-n}{m}\,\alpha + R_k\right) - \theta\left(\zeta - \frac{2-n}{m}\,\alpha - R_k\right)\right], \tag{21}$$

and

$$R_k = \left\{\alpha^2 + \tfrac{1}{4}\left[(2-n)^2 - m^2\right]\epsilon_k^2\right\}^{1/2}. \tag{22}$$

Equations (16)–(18) define a system of three equations in three unknowns with one parameter. These equations may be decoupled by choosing n as the parameter and introducing a new variable $Z_{1\lessgtr 1}$ which is equal to the value of ϵ_k at which there is the discontinuity in one of the two heaviside unit functions for a given ζ, m, and the parameter n. The discontinuity appears in one or the other, depending on whether $X_1 < \frac{1}{2}$ or $X_1 > \frac{1}{2}$. The new set of variables are m, α, and Z with n as the parameter. If now Eqs. (16) and (17) are inverted

$$X_1 = \left[n(2-n) - m^2\right]/\left[(2-n)^2 - m^2\right], \tag{23}$$

$$X_2 = 2m(1-n)/\left[(2-n)^2 - m^2\right]. \tag{24}$$

Equation (23) determines Z as a function of m. Then Eq. (18) will give α as a function of m; and finally Eq. (24) gives m.

The solutions for the sublattice magnetizations are plotted in Figs. 8 and 9 for the sc and bcc lattice structures, respectively. There are two antiferromagnetic solutions as was indicated by the susceptibility results. In contrast with the ferromagnetic solutions, the curve corresponding to the larger sublattice magnetization does not saturate except at $n = 1$. That there are no saturated solutions for $n < 1$ is a general result for the model within the two-pole approximation and does depend on the particular density of states. This can be seen by substituting $n = m$ in Eqs. (23) and (24) to find $X_1 = X_2$, while by their definitions (19) and (20) it follows that $X_2 < X_1$ for $n < 1$.

V. ENERGY

A calculation of the energy per site for each configuration gives

$$E_F = \tfrac{1}{2}N^{-1}\sum_{k\sigma}(1-\bar{n}_{-\sigma})\left[(2-n_{-\sigma})\,\epsilon_k + E_{-\sigma}\right] \times \theta\left(\zeta - \left[E_{-\sigma} + (1-\bar{n}_{-\sigma})\epsilon_k\right]\right) \tag{25}$$

for the ferromagnetic phase and

$$E_A = (X_1 + \tfrac{1}{2}n - 2)\,(\alpha/2m)\left[(2-n)^2 - m^2\right] \tag{26}$$

for the antiferromagnetic phase. These expressions are valid only when the number of electrons is less than the number of sites. However, since the energy per site for the model with $\bar{n}_{\sigma}$ holes is given by

$$E(\bar{n}_{\sigma}\ \text{holes},\ t) = E(\bar{n}_{\sigma}\ \text{electrons},\ -t) + \tfrac{1}{2}I(n-1), \tag{27}$$

where the first term on the right-hand side of Eq. (27) denotes the energy per site for the model with the transfer energy t replaced by $-t$, Eqs. (25) and (26) are sufficient to determine the energy even when $n > 1$.

The paramagnetic and lowest ferromagnetic and antiferromagnetic energies are plotted as a func-

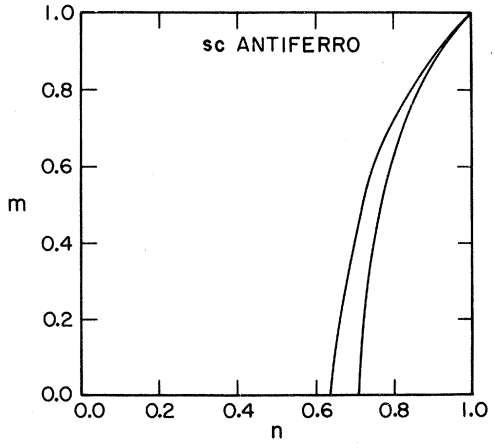

FIG. 8. Sublattice magnetization per site at absolute zero as a function of electron concentration for the simple-cubic lattice.

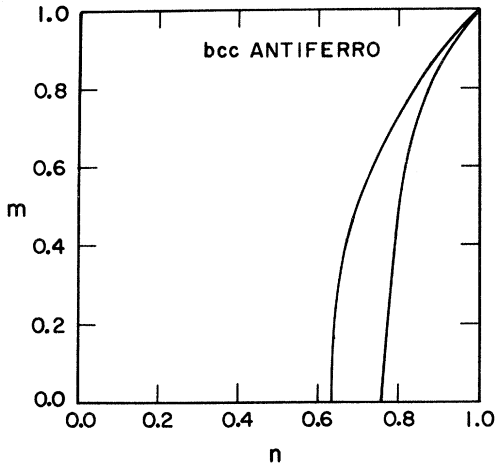

FIG. 9. Sublattice magnetization per site at absolute zero as a function of electron concentration for the body-centered-cubic lattice.

tion of the number of electrons per site in Figs. 10 and 11 for the sc and bcc structures, respectively. The ferromagnetic solution of lowest energy corresponds to the solution of larger magnetization. The other ferromagnetic solution has an energy between this ferromagnetic solution and the paramagnetic solution. In the antiferromagnetic case the energy corresponding to the solution of lesser sublattice magnetization lies slightly above the paramagnetic solution, while the energy of the other solution lies slightly above the first magnetic solution. In Fig. 12 are plotted the curves for the

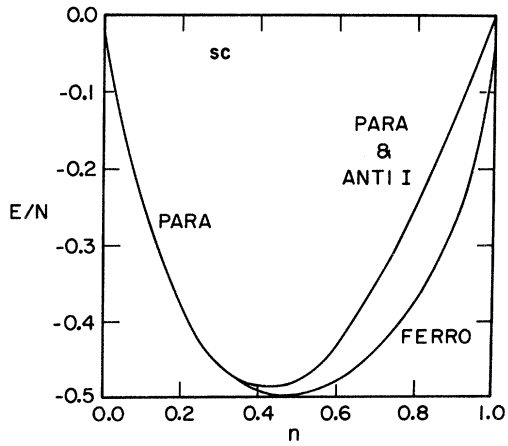

FIG. 10. Energy per site at absolute zero as a function of electron concentration for the simple-cubic lattice. The curve marked PARA is the paramagnetic energy. The lowest-energy antiferromagnetic configuration is labeled ANTI, and the lowest-energy ferromagnetic configuration is labeled FERRO. The scale of energy is such that the transfer energy between states at neighboring sites is $-\frac{1}{2}$.

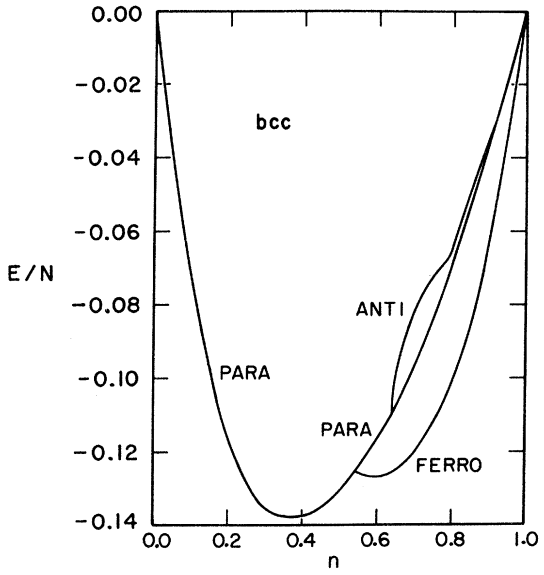

FIG. 11. Energy per site at absolute zero as a function of electron concentration for the body-centered-cubic lattice. The curve marked PARA is the paramagnetic energy. The lowest-energy antiferromagnetic configuration is labeled ANTI, and the lowest-energy ferromagnetic energy is labeled FERRO. The scale of energy is such that the transfer energy between states at neighboring sites is $-\frac{1}{8}$.

paramagnetic and both ferromagnetic energies of the fcc lattice. Again the ferromagnetic solution of larger magnetization gives the lowest energy.

VI. DISCUSSION

The two-pole approximation of Roth[1] is an improved version of the first Hubbard theory[3] for the narrow-s-band model. It is obviously an improvement for the study of the magnetic properties since it includes a band shift that makes ferromagnetism more likely in the nearly-half-filled-band case for simply-shaped densities of states. The work of Harris and Lange[8] shows that this spin-dependent shift is implicit in the model. Furthermore, two known deficiencies of the two-pole approximation are probably not serious when one examines the possibility of ferromagnetism. One, the approximation does not give the Kanamori[9] results at low density; however, one only expects instabilities of the paramagentic state at higher electron concentrations. Two, it shares with the Hubbard[3] theory the defect that the single-particle spectrum has a gap for any finite I, no matter how small; however, nonparamagnetic phases are likely to occur only when I is the order of the bandwidth or greater, in which case one may expect a gap in the single-particle spectrum.

A novel feature of the two-pole approximation is the appearance of two solutions for both the ferro-

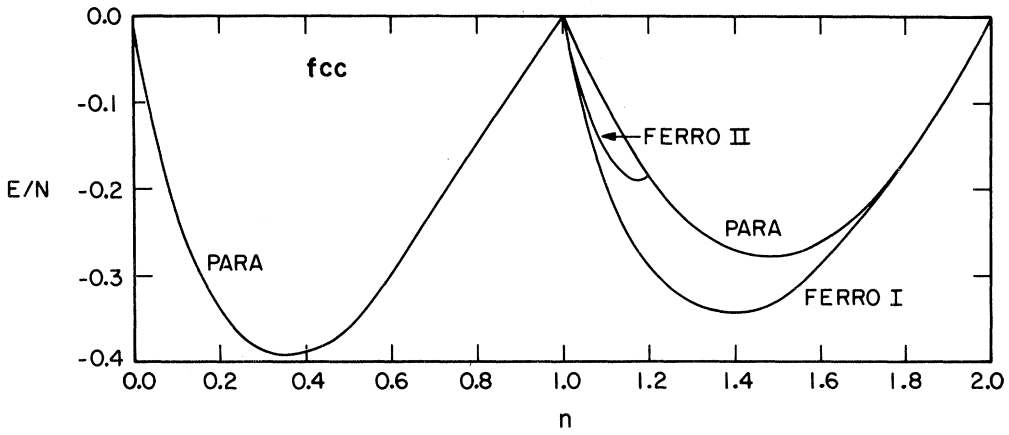

FIG. 12. Energy per site at absolute zero as a function of electron concentration for the face-centered-cubic lattice. The curve marked PARA is the paramagnetic energy. The curve labeled FERRO I is the energy of the saturated configuration, and the curve labeled FERRO II is the energy of the configuration of smallest non-zero magnetization. For $n>1$ the energies plotted are $E/N-\frac{1}{2}I(n-1)$. The scale of energy is such that the transfer energy between states at neighboring sites is $-\frac{1}{4}$.

magnetic and antiferromagnetic phases. The physical origin of the two solutions is associated with the gap in the single-particle spectrum. (In fact, such a situation can arise in the original Hubbard[3] theory.) It is believed that this is a real feature inherent in the model and not an artifice of the approximation used.

For I infinite there are certain exact results for nearest-neighbor band structures, as considered in this paper. These results, due to Nagaoka,[2] can be summarized as follows. When the band is nearly half-filled (i.e., the number of electrons is slightly less than the number of sites), the ferromagnetic state with maximum total spin is the ground state for sc and bcc crystal structures, while for fcc crystal structures the maximum total spin ferromagnetic state is or is not the ground state, depending on whether the number of electrons is greater or less than the number of sites. Note that our results based on the two-pole approximation are in complete agreement with the conclusion of Nagaoka.[2]

For exactly one electron per site and an infinite I, the energy per site must vanish rigorously for all magnetic configurations. The two-pole approximation is seen to give this result for the phases studied. With one electron per site and I large but finite, the antiferromagnetic state has a lower energy than the ferromagnetic state.[10] Unfortunately, since our calculations are for $I=\infty$, there is no indication from our work whether the two-pole approximation will give the relative energies correctly when I is finite and the number of electrons per site is one.

In the present investigation we considered only the case where I is infinite. This affords a considerable simplification since one need consider excitation energies corresponding to only one of the two subbands resulting from the splitting of the unperturbed band due to the Coulomb term. Also, one has the greatest confidence in the two-pole approximation when I is infinite since certain two-particle correlation functions involving a double occupancy vanish rigorously and one need not find approximate expressions which are of uncertain validity. The results we have obtained for the case of infinite I confirm by their agreement with the exact conclusions of Nagaoka[2] this confidence in the Roth[1] approximation. This fact indicates that it would now be of interest to attempt an extension of these results to finite I so that one could make comparisons with the Hartree-Fock-type analysis by Penn[11] and the t-matrix analysis by Caron and Kemeny,[12] as well as the more recent functional integration methods. We intend to make such a study in the future.

*Supported in part by the National Science Foundation under Grant No. GP 20645.

[1]L. M. Roth, Phys. Rev. **184**, 451 (1969).
[2]Y. Nagaoka, Phys. Rev. **147**, 392 (1966).
[3]J. Hubbard, Proc. R. Soc. A **276**, 238 (1963).
[4]D. N. Zubarev, Usp. Fiz. Nauk **73**, 71 (1960) [Sov. Phys.-Usp. **3**, 320 (1960)].
[5]D. H. Faulkner and J. W. Schweitzer, J. Phys. Chem. Solids **33**, 1685 (1972).
[6]J. W. Schweitzer and J. D. Maynard, Jr., Phys. Rev. B **3**, 2357 (1971).
[7]R. J. Jelitto, J. Phys. Chem. Solids **30**, 609 (1969).
[8]A. B. Harris and R. V. Lange, Phys. Rev. **157**, 295 (1967).
[9]J. Kanamori, Prog. Theor. Phys. **30**, 276 (1963).

[10]C. Herring, in *Magnetism*, edited by G. Rado and H. Suhl (Academic, New York, 1966), Vol. IV, p. 212.
[11]D. R. Penn, Phys. Rev. **142**, 350 (1966).
[12]L. G. Caron and G. Kemeny, Phys. Rev. B **4**, 150 (1971).

PHYSICAL REVIEW B VOLUME 7, NUMBER 9 1 MAY 1973

Low-Temperature Structure of $PbTiO_3$†

P. Doshi, J. Glass, and M. Novotny
Department of Physics, North Dakota State University, Fargo, North Dakota 58102
(Received 19 October 1972)

Measurements of the perturbed γ-γ directional correlation have been made for the first excited state of ^{44}Sc in polycrystalline lead titanate at $-(189\pm5)$ °C. A static electric quadrupole interaction was observed, having an interaction strength $|QV_{zz}|=(4.09\pm 0.09)\times10^{-8}$ V, which is greater than the value obtained at room temperature by a factor of 1.04 ± 0.02. The field gradient at the ^{44}Sc-ion site is found to have axial symmetry, indicating a tetragonal structure for lead titanate at -189 °C. The axial ratio at this temperature is estimated to be 1.108 ± 0.027, which agrees well with recent x-ray studies indicating a new tetragonal phase formed by a transition at -160 °C. Using a recently reported value of γ_∞ (Sc^{3+}), the quadrupole moment of the 68-keV state in ^{44}Sc is found to be (0.109 ± 0.020) b. Using this number it is shown that the room-temperature values of field gradient observed with ^{44}Sc and ^{57}Fe probes differ by a factor of 16.5.

I. INTRODUCTION

Lead titanate $PbTiO_3$ is ferroelectric at room temperature and has a Curie temperature of 490 °C, highest known among the perovskite-type ferroelectrics. In recent years much work[1-6] has been done on the structure and properties of $PbTiO_3$ and its solid solutions from room temperature up to 600 °C. It has been many years, however, since most studies have been made of the low-temperature structure of this ferroelectric.

The permittivity of $PbTiO_3$ ceramic was first measured by Shirane and Hoshino[7] over a temperature range of -170 to 580 °C. These measurements indicated only one structural transition, in sharp contrast to $BaTiO_3$ in which three transitions occur. An x-ray diffraction study from 30 to 535 °C indicated a tetragonal structure below the Curie point, but showed a decreasing axial ratio and unit-cell volume with increasing temperature. This was attributed to the temperature dependence of a strong polarization. In later works, Kobayashi, Ueda, and Okamoto[8,9] performed an x-ray study and measured the dielectric constant for $PbTiO_3$ powder samples in the temperature range of 40 to -150 °C. The x-ray data showed a distinct transition at -100 °C, with an associated increase in the negative volume expansion coefficient and the appearance of superlattice lines. The new phase of $PbTiO_3$ below -100 °C was interpreted as a superstructure in which oxygen ions in different sublattices are considerably displaced in antiparallel directions. This, combined with the negative value of the volume expansion coefficient, strongly suggests that $PbTiO_3$ transforms into an antiferroelectric structure at -100 °C. This transition, however, could only be observed if the sample was cooled or heated very slowly at a rate of 0.3 °C/min. The dielectric-constant data showed a slow change in temperature dependence around -60 °C and anomalies at -100 and -150 °C, but due to experimental difficulties no x-ray data were taken at -150 °C. A detailed report has recently been given[10] on x-ray, thermal, and piezoelectric studies of the low-temperature phase transitions. X-ray measurements from 26 to -192 °C have indicated a possible transition to a new tetragonal phase at around -160 °C. Differential thermal analyses showed anomalies at -160 °C, but not at -100 °C. From measurements of the electromechanical coupling factor of the longitudinal length extensional mode, the authors have concluded that the two low-temperature phases at around -100 and -160 °C are not antiferroelectric. No superlattice lines were observed below -100 °C in this study.

The techniques of perturbed γ-γ directional correlations (PDC) and Mössbauer spectroscopy (MS) have recently been used to probe fields at the Ti^{4+}-ion site in both $BaTiO_3$ and $PbTiO_3$ at room temperature.[11-14] The field gradients observed are axially symmetric and have magnitudes in $PbTiO_3$ greater than those in $BaTiO_3$ by a factor of 1.41 ± 0.04 (MS) or 1.46 ± 0.07 (PDC). A comparison of field-gradient values obtained by these two techniques will be made later in this paper. We wish to report here the application of PDC to the measurement of the electric field gradient at the titanium-ion site in $PbTiO_3$ at liquid- nitrogen temperature.